Detailed seismic bathymetry beneath Ekström Ice Shelf, Antarctica: Implications for glacial history and ice-ocean interaction

Emma C. Smith[1], Tore Hattermann[2], Gerhard Kuhn[1], Christoph Gaedike[3], Sophie Berger[1], Reinhard Drews[4], Todd A. Ehlers[4], Dieter Franke[3], Raphael Gromig[1*], Coen Hofstede[1], Astrid Lambrecht[5], Andreas Läufer[3], Christoph Mayer[5], Ralf Tiedemann[1,6], Frank Wilhelms[1,7], Olaf Eisen[1,6]

[1]Alfred-Wegener-Institut Helmholz-Zentrum für Polar- und Meeresforschung, Bremerhaven, Germany
[2]Norwegian Polar Institute, Tromsø, Norway
[3]BGR, Federal Institute for Geosciences and Natural Resources, Geozentrum Hannover, Hannover, Germany
[4]Department of Geosciences, University of Tübingen, Tübingen, Germany
[5]Geodesy and Glaciology, Bavarian Academy of Sciences and Humanities, Munich, Germany
[6]Department of Geosciences, University of Bremen, Bremen, Germany
[7]Department of Geosciences, University of Göttingen, Göttingen, Germany

Key Points:

- Seismic vibroseis surveys used to map of ice-shelf cavity beneath Ekström Ice Shelf in Antarctica
- Deep trough and overdeepenings are evidence of past ice streaming and retreat along retrograde slope
- Existence of two ocean circulation regimes in the shallow and deep parts of the cavity

*Now at: Max Planck Institute for the Science of Human History, Jena, Germany

Corresponding author: Emma C. Smith, emma.smith@awi.de

Abstract

The shape of ice-shelf cavities are a major source of uncertainty in understanding ice-ocean interaction and limit our assessment of the response of the Antarctic ice sheets to climate change. Here we use seismic reflection vibroseis data to map, with unprecedented detail, the bathymetry beneath the Ekström Ice Shelf, Dronning Maud Land. The new bathymetry reveals an inland-sloping trough, reaching depths of 1100 m near the current grounding line, which we attribute to a palaeo-ice stream. The trough does not cross-cut the continental shelf. Conductivity-temperature-depth profiles within the ice-shelf cavity reveal the presence of cold water at shallower depths with clear tidal mixing at the ice-shelf margins. It is unknown if warm water is present in the trough, although it has been observed in a similar trough under a neighbouring ice shelf. These similarities suggest this bathymetry is characteristic of Dronning Maud Land ice shelves.

Plain Language Summary

Antarctica is surrounded by floating ice shelves, which play a crucial role in regulating the flow of ice from the continent into the oceans. The ice shelves are susceptible to melting from warm ocean waters beneath them. In order to better understand the melting, knowledge of the shape and depth of the ocean cavity beneath the ice shelves is crucial. In this study we present new measurements of the sea floor depth beneath Ekström Ice Shelf in East Antarctica. The measurements reveal a much deeper sea floor than previously known. We discuss the implications of this for oceanic access to the base of the ice shelf and discuss how the observed sea-floor features could have been formed by historical ice flow. Although Ekström Ice Shelf is relatively small, the deep sea floor found here is thought to be representative of many small ice shelves in this region, which together regulate the ice loss from a large area of East Antarctica.

1 Introduction

Ice shelves surrounding Antarctica act as buttresses, restraining ice discharge from the continent into the oceans and therefore regulating Antarctic contributions to sea-level rise (Dupont & Alley, 2005). Mass loss from Antarctica has been accelerating over the past 20 years (IPCC, 2019), driven by increased basal melting of ice shelves (Paolo et al., 2015; Pritchard et al., 2012). Accurate knowledge of the bathymetry of the ice-shelf cavity is essential for understanding processes active at the ice-shelf ocean interface. Recent studies have highlighted a lack of sub-shelf bathymetry as a "major limitation" (Pattyn et al., 2017) for future projections of Antarctic mass balance and a "leading factor" (Goldberg et al., 2019) in model and data disagreement. Improved bathymetric mapping allows determination of water access pathway and calculation of spatially and temporally variable melt rates (e.g. Tinto et al. (2019); Cochran et al. (2014); Milillo et al. (2019)). In addition, sub-ice shelf bathymetry also provides information about ice-dynamic history of the region. Understanding the past ice dynamics and implementing an accurate bathymetry in ice-flow and oceanographic models will lead to improved projections of the evolution of the ice-sheet.

The coast of Dronning Maud Land (DML), East Antarctica (Fig.1) is fringed by many small ice shelves. In this area satellite-derived melt rates are typically low (Rignot et al., 2013). The continental shelf in this area is narrow, meaning the ice shelves in the region are in close proximity to Warm Deep Water (WDW) masses (Nøst et al., 2011), making this a potentially sensitive region to future change (Heywood et al., 1994; Hattermann, 2018; Thompson et al., 2018). In addition, the ice shelf-ocean interactions along the DML coast play an important role in preconditioning the structure and water-mass properties of the westward flowing boundary current (Hattermann, 2018; Fahrbach et al., 1994). This current is a key control on warm-water inflow toward the Filchner Ronne Ice Shelf (Hellmer et al., 2017; Timmermann & Hellmer, 2013) and takes part in bot-

tom water formation in the Southern Weddell Sea (Meredith et al., 2011; Meijers et al., 2016).

The Ekström Ice Shelf (Fig.1) is one such ice shelf, covering an area of approximately 6800 km^2 (Neckel et al., 2012). It is laterally constrained by the grounded ice rises of Søråsen to the west and Halvfarryggen in the east (Fig. 1). The present ice-shelf front is less than 20 km from the continental shelf break. Until now, little was known about the bottom topography of the ice shelf cavity. A number of seismic reflection measurements by Kobarg (1988), suggest the southward deepening of the seafloor with a maximum water column thickness of 500 m under the center of the ice shelf. However, this dataset was not archived and a map of the cavity is currently lacking. The satellite derived average basal melt rate for the Ekström Ice Shelf is 1.1 m (S. Berger, personal communication, 2019 - method of Berger et al. (2017)). This value is slightly larger than the rates measured under the neighbouring Nivl (Lindbäck et al., 2019) and Fimbul (Hattermann et al., 2014) ice shelves. There is indication that a significant amount of super-cooled water is produced in the Ekström Ice Shelf cavity, which interacts vigorously with the waters in the adjacent Atka Bay, forming large amounts of platelet ice beneath the landfast sea ice there (Hoppmann et al., 2015). Under the neighbouring Fimbul ice shelf, a previously unknown deep trough within the sub-shelf cavity was discovered (Nøst, 2004) and confirmed to contain modified WDW (Hattermann et al., 2012, 2014), highlighting the need for accurate bathymetry measurements in these regions.

Access to the sub-shelf cavity has previously been challenging with radar systems, because of difficulties in penetrating through the water column. Similarly, sub-shelf cavities have rarely been explored with AUVs (autonomous underwater vehicles) because they require ship support for deployment (e.g. Nicholls et al. (2006)). Here, we present a new detailed map of the ice-shelf cavity and sea-floor bathymetry beneath the Ekström ice shelf. We use an extensive grid of new and existing seismic reflection data. These data were collect from the ice-shelf surface, using a specialised vibroseis seismic source and snow streamer system (Eisen et al., 2015). We integrate the bathymetric mapping with conductivity-temperature-depth (CTD) data acquired through hot-water-drilled boreholes in the ice shelf and under sea ice in Atka Bay. The combined observations are used to identify the primary implications of this new bathymetry for ice-ocean interaction and the ice-dynamic history in the region.

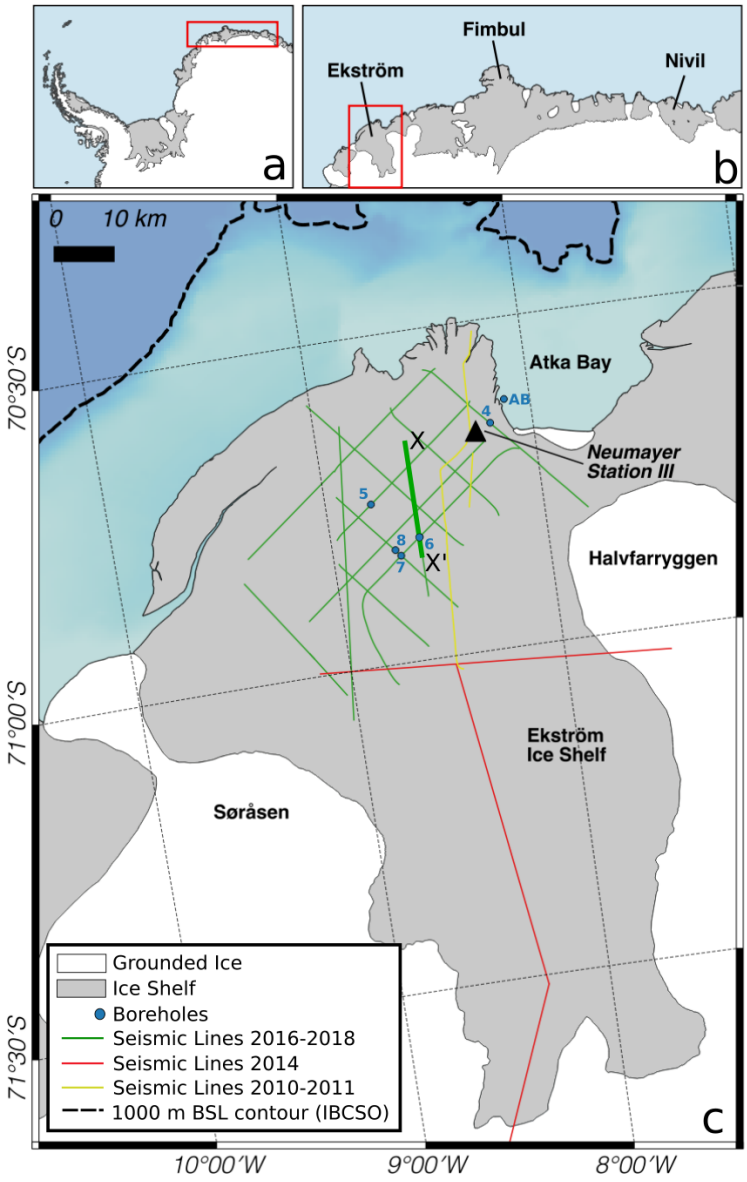

Figure 1. a) Location of Dronning Maud Land within Antarctica b) Area highlighted in (a) with location of Ekström ice shelf indicated and c) Ekström ice shelf with seismic survey data and boreholes shown. In all figures the ice shelf is shown in grey and grounded ice in white. In (c) The ocean background is the international bathymetric chart of the Southern Ocean (IBCSO) (Arndt et al., 2013), with the 1000 m below sea level contour shown as a dashed line. The borehole names are shorted for display purposes, for example '4' refers to borehole 'EIS-4' and 'AB' to 'Atka Bay'. The location of the seismic line Fig. 2 is X- X' .

2 Data and Methods

2.1 Seismic Data Acquisition

The seismic data used to map the bathymetry of the sea floor beneath the ice shelf were collected between 2010 and 2018, using two different seismic vibroseis sources. The same snow streamer was used for all data acquisition and was 1500 m long, containing 60 channels, with a 25 m group spacing. Each group contains eight gimballed P-wave SM-4, 14 Hz geophones. For all data collection the vibroseis source was towed behind a snow tractor with the snow streamer towed behind that. At each shot point several vibroseis sweeps were made, to allow shot stacking for increased signal-to-noise ratio. This method of operation allowed for high data acquisition rates of around 20 km per day for 6-10 fold data. A more detailed explanation of both these seismic sources, the snow streamer and the operational method is given by Eisen et al. (2015).

The main grid of data, at the ice shelf front, was collected during the 2016/17 and 2017/18 austral summers (Fig.1, green) as part of the Sub-EIS-Obs project (Kuhn & Gaedicke, 2015), using the AWI IVI EnviroVibe source, producing a 10 second linear sweep from 10-220 Hz. These data are high fold (6-15) with the exception of the two lines the north western corner of the grid and are single fold. It was not possible to extend data collection further to the west due to surface crevassing. The seismic lines extending across the grounding line to the east and south were collected in 2014 (Fig.1, red), using the same acquisition configuration, and are single fold. Three older lines from 2010 and 2011 overlap the main grid (Fig.1, yellow) and were acquired using the University of Bergen Failing Y-1100 vibroseis source (Kristoffersen et al., 2014), with a 10 second sweep from 10-100 Hz; fold varies between 1 and 8.

All seismic data were processed for this study, to ensure consistent treatment of data from different surveys (Supporting Information S1). The resulting seismic time-stacked sections all have clear ice base and the sea floor reflections (Fig. 2). The travel-time of these reflections were hand-picked on each section.

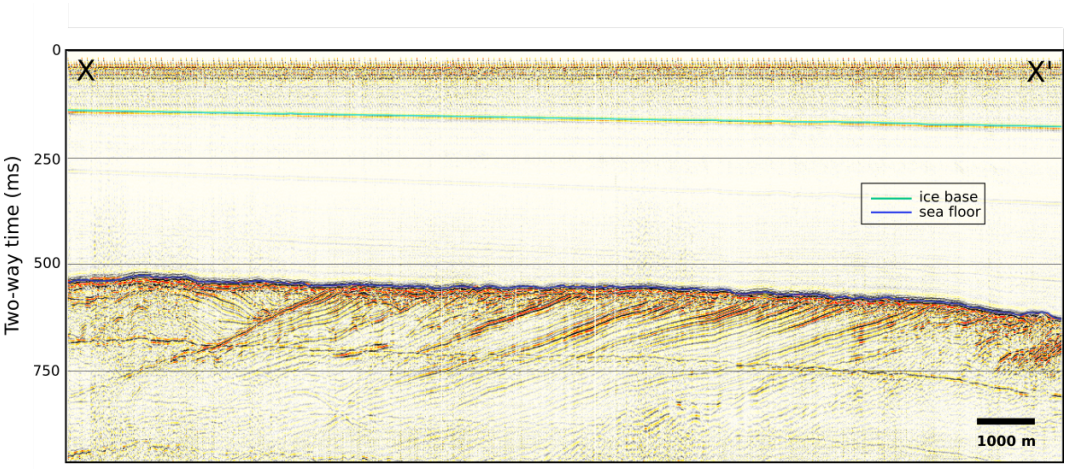

Figure 2. Example of a seismic time-stacked section. Location of section is marked X-X' on Fig. 1, AWI line number 20170561. Reflections from the ice base and sea floor are clearly visible and the travel-time to them can be easily picked. The section is vertically exaggerated by a factor of 10

2.2 Depth Conversion and Gridding of Seismic Data

The hand-picked travel times from all seismic lines were used to create grids of the travel-time to the ice base and sea floor, using a krigging algorithm. Any mis-ties between picks, in areas where seismic lines overlap, were handled by assigning priority to the higher resolution surveys. Each grid was then depth converted using a seismic velocity 3601 ms^{-1} for ice and 1451 ms^{-1} for the water column. The final step was to correct the depth of each grid for the ice surface elevation, using the REMA digital elevation model v1.1 (Howat et al., 2019), which was re-referenced to the GL04C geoid (Förste et al., 2008).

The seismic velocity used for depth conversion of the ice was derived from the average stacking velocity V_{stack}, determined during velocity analysis (Supporting Information S1). The value of V_{stack} can be assumed to equal the interval velocity (V_{int}) for ice, as it is a quasi-homogenous layer and the reflection is from a near-horizontal surface (base of the ice shelf). The depth-averaged seismic velocity value for the water column was determined using CTD profiles (see Section 2.4) taken through the hot-water drilled boreholes. The TEOS-10 Matlab toolbox (IOC et al., 2010; McDougall & Barker, 2011) was used to make the calculation. The resulting value is comparable to values determined from CTD data under other Antarctic ice shelves (Nøst, 2004; Brisbourne et al., 2014; Rosier et al., 2018).

2.3 Uncertainties in Bathymetry

Uncertainties in the sea-floor depth come from four main sources: (i) accuracy of the horizon picking, (ii) velocities used for depth conversion of these horizons, (iii) errors in the REMA DEM used for surface elevation corrections and (iv) depth errors from unmigrated data. A detailed analysis of these individual error sources was made (Supporting information S2), resulting in cumulative error at the sea floor of $\pm$ 14.8 m in the main data grid and $\pm$ 34.4 in the areas of the 2014 seismic lines, which extend from the main grid towards the grounding lines (Fig. 1).

It was possible to measure the ice thickness and sea-floor depth at the five borehole locations (Fig. 1) on the ice shelf, both during drilling and also subsequently with camera equipment and coring devices deployed through the boreholes to the sea floor. These measurements confirmed the seismic determined ice thickness was within $\pm$ 5 m of the measured thickness and the sea floor to within $\pm$ 10 - 20 m. This validates our error estimates, as the latter range also includes bending of the sampling rope by tidal currents.

2.4 CTD Data

During the 2018/19 austral summer, hot-water-drilled boreholes were made at five locations on the ice shelf. An RBR Concerto conductivity-temperature-depth (CTD) sensor was repeatedly lowered through each borehole and through a sea-ice lead in Atka Bay (Fig. 1). The CTD sensor recorded water mass properties at a frequency of 1 Hz. These data were used to calculate seismic velocities for depth conversion of the sea-floor seismic reflection (see Section 2.2) and to determine the source of water masses present beneath the ice shelf and sea ice.

CTD data were processed using the RBR Ruskin software, which was used to export pressure, in-situ temperature and practical salinity data based on the sensor calibration that was obtained in October 2018 before the field season. Afterwards, the CTD profiles were split into individual down casts and up casts at each location and all data were inspected manually. Profiles showing obvious sensor drift and noise, as is often related to temporary accretion of ice crystals inside the conductivity cell in these environments, were discarded. The remaining data showed a plausible water mass distribution

beneath the ice shelf, but since no post calibration of the sensor after the field season was available, a larger nominal uncertainty is assumed for the obtained in situ temperature (0.01°C) and practical salinity (0.03) values.

3 Results and Discussion

The new bathymetry (Fig. 3a) is independent of any previously available products of ice thickness or water depth. Here, we compare the new bathymetry to Bedmap2 (Fretwell et al., 2013) bed topography (Fig. 3b), which is the baseline dataset for the large majority of modelling studies. We highlight the differences to emphasise the need for dedicated measurements of sub-ice shelf bathymetry. The new data reveals significant, previously unknown, bathymetry beneath the Ekström Ice Shelf.

The Bedmap2 topography under Ekström Ice Shelf is relatively uniform, deepening towards the grounding line (Fig. 3b). Looking at cross sections through the region (Fig. 3c) it is clear that this bathymetry is not realistic, given that it is largely following the ice shelf base. However, this is unsurprising given the lack of previously available data (Fretwell et al., 2013) and similar mismatches have been document for other ice shelves in this sector (e.g. Nøst (2004); Favier et al. (2016)).

Beneath the main grid of our data (Fig. 3a) we find a bathymetric trough under the central part of the ice shelf, which appears aligned with the ice-flow direction. In this area the trough is 30 km wide and reaches depths of up to 800 m below sea level (Figs. 3a and 3c, C-C'). It is flanked by shallower plateaus to the sides, at around 450-500 m depth (Figs. 3a and 3c, C-C' and D-D') and shallows to around 300 m depth at the marginal grounding lines joining the ice shelf to the ice rise of Halvfarryggen (Figs. 3a and 3c, B-B'). The shallowing topography seen in the west of the grid, suggests that the cavity shape seen in the east is mirrored to the western grounding line at Søråsen. The sea floor directly in front of the ice shelf is at 450 m depth, a similar depth to the plateau flanking the trough. A basin-like depression, around 570 m deep, is seen on the eastern plateau, to the south of Neumayer station. A profile from in front of the ice-shelf edge to the current grounding line, following the trough under the main grid and the single seismic line connecting the south of the grid to the grounding line, indicates an inland sloping sea floor (Figs. 3a and 3c, A-A'), reaching a maximum depth of 1100 m around 10 km downstream of the current grounding line.

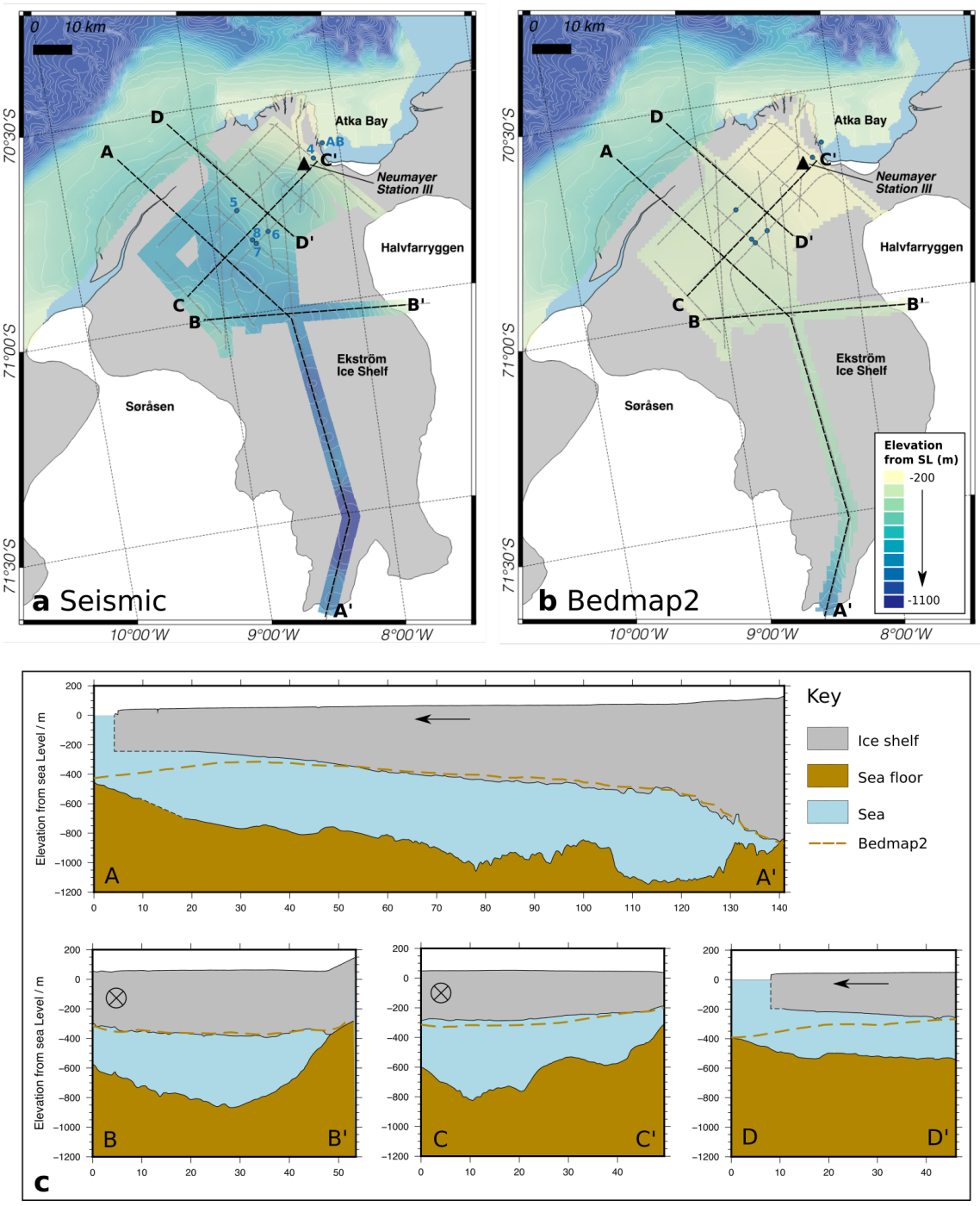

Figure 3. a) Gridded sea-floor bathymetry beneath the Ekström Ice Shelf, derived from seismic measurements (this study), bathymetry seawards of the ice-shelf edge is from the IBCSO (Arndt et al., 2013) mapping project and is cut to area where measurements are present. White contours are at 50 m intervals. Grey dashed lines show the seismic data locations, with the cross sections show in (c) indicated by black dashed lines. Blue points indicate the location of hot water drilled boreholes as in Fig. 1. b) As in (a) but with sub-ice shelf bathymetry from Bedmap2 (Fretwell et al., 2013) co-located with seismic bathymetry. c) Cross sections of the ice-shelf cavity and sea floor beneath and in front of Ekström Ice Shelf. Ice flow direction is indicated by arrows and cross-hairs. Sea-floor bathymetry (brown) is from the seismic grid merged with IBSCO, seaward of the ice-shelf edge. The ice shelf (grey) is derived from gridded seismic data at the ice base and REMA surface elevation. Solid black out-lines are areas where data is present, dashed lines in A-A' and D-D' are data gaps. The ocean is shown in blue. Bedmap2 elevations are show as brown dashed lines for comparison. All data is referenced to the GL04C geoid

3.1 Ice-Ocean Interaction

The newly mapped ice shelf cavity has implications for how the ocean may affect ice-shelf and grounded ice in the Ekström region. The largest potential source of ocean heat, available for ice shelf melting, is provided by the WDW that circulates as part of the Antarctic Slope Front along the continental slope (Heywood et al., 1994). Prevailing easterly winds suppress the WDW several hundred meters below sea level in this 'fresh shelf' region (Thompson et al., 2018). The deeper trough beneath the central part of the ice shelf does not cross-cut the continental shelf. This means WDW access to the cavity is limited, explaining the relatively low basal melt rates. This is confirmed by the CTD profiles taken within the cavity (Fig 4), which show relatively cold water with maximum in-situ temperatures close to the surface freezing point (-1.9 °C) and maximum practical salinity around 34.4, which is the characteristic signature of the Eastern Shelf Water (ESW) that resides above the WDW in this region (Fig. 4). The deeper trough, however, constitutes a conduit along which denser open-ocean water, could enter the cavity and reach the deeper grounding line (Fig. 3c, A-A'). In particular, if WDW enters the cavity over the shelf break, the several hundred meters of water column thickness will allow for three-dimensional overturning circulation. In this scenario, near-bottom inflows of WDW can propagate towards the grounding line, undiluted by colder buoyant outflows that are observed to exit the cavity at shallower depths along the ice shelf base (Fig. 4a).

Intermittent warmer inflows have been observed beneath the neighbouring Fimbul Ice Shelf (Hattermann et al., 2012). We do not find these inflows in the temporal snapshots of our CTD profiles under Ekström, that were taken over the shallower slopes in the northern part of the cavity. It is, however, likely that a slightly warmer bottom layer, similar to what was observed at the deepest site beneath the Fimbul Ice Shelf (Fig. 2b in Hattermann et al. (2012)), fills the southern parts of the trough beneath the Ekström Ice Shelf. Comprising only mediocre local maxima at the depth of the present grounding line position, the emergent bathymetry along the central cross section (Fig. 3c, A-A') therefore renders the ice shelf vulnerable to any changes in the slope front configuration, that may bring WDW above the depth of the shelf break. This has been suggested as a response to future climate change in this region (Hellmer et al., 2017; Hattermann, 2018).

Furthermore, our observed seafloor bathymetry suggests a separation of different circulation regimes beneath the ice shelf. While the central part of the cavity seems to be dominated by the trough system; the eastern portion of the ice shelf, adjacent to Atka Bay, comprises a zone of relatively thin water column (Figs. 3a and 3c, C-C') that is likely subjected to intense tidal mixing. The interaction of tides with buoyant outflows, rising along the eastern flank of the ice shelf in this region, may be responsible for the vigorous accretion of marine ice that is being observed beneath the fast ice in Atka Bay. Hoppmann et al. (2015) found that platelet ice crystals leave the ice shelf cavity in intermittent pulses, that may be linked to tides. The temperature profiles from the EIS-4 site confirm the existence of a tidally mixed zone in this region. The EIS-4b profile shows a similar vertical gradient in temperature to the profiles obtained in the deeper part of the cavity. However, the EIS-4i profile, taken around 11 hours later than EIS-4b, at the same location, has a much more homogeneous vertical temperature structure. According to the CATS regional tidal model (Padman et al., 2008), a tidal cycle of ∼1 m amplitude passed the EIS-4 borehole location between the two measurements. This is approximately twice as large as the tidal cycle that passed the borehole 12 hours prior to the first measurement (EIS-4b). Similar tidal flushing events that mix the entire water column may be responsible for mixing larger volumes of potentially super-cooled ice shelf water in shallower depths, where they contribute with platelet ice formation to the fast ice morphology in Atka Bay.

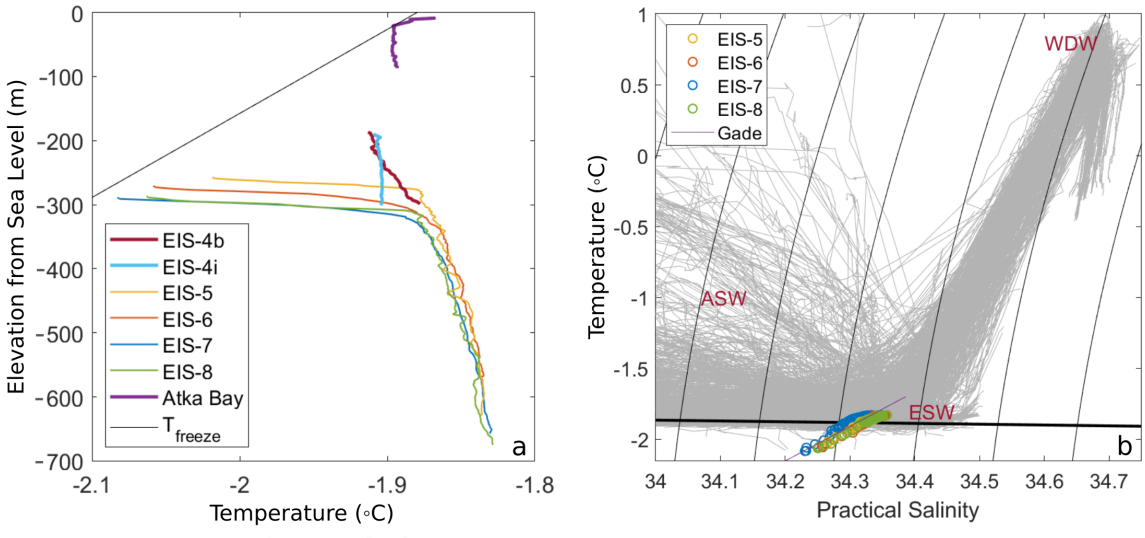

Figure 4. Vertical CTD profiles taken through boreholes (location Fig. 3) (a) In-situ temperature observed at different sites beneath Ekström Ice Shelf and beneath the fast ice in Atka Bay. The black line indicates the pressure-dependent melting point temperature for a given practical salinity of 34.25. Distribution (b) of in-situ temperature and practical salinity profiles at the sites where reliable salinity measurements could be obtained. Gray profiles show the regional subset of open ocean CTD profiles presented in Hattermann (2018), indicating ambient water masses with abbreviation indicating the end members of Warm Deep Water (WDW), Eastern Shelf Water (ESW) and Antarctic Surface Water (ASW). The purple line shows the melt water mixing line along which a given water mass may transform through interaction with the ice shelf (Gade, 1979) when assuming zero conductive heat flux into the ice. Black curves indicate horizons of constant density, the thick black line indicates the melting point temperature at surface pressure.

3.2 Ice-Dynamic History

The sea floor bathymetry under Ekström Ice Shelf enhances our understanding of past ice extent and retreat in this region. The deepened trough under the centre of the Ekström Ice Shelf is interpreted as a relict landscape formed through erosion by former ice streams. Under the main grid it is 300-400 m deeper than the surrounding sea-floor plateau (Fig. 3a). Due to a ∼10 km data gap, it is not certain how the trough shallows between the end of the seismic grid and the IBCSO sea-floor data at the ice-shelf front. However, at the ice-shelf front the sea floor is at the same depth as the plateau under the ice shelf (450 m) and the trough does not cross-cut the continental shelf. This could indicate ice flow in this trough slowed in the area of the current ice-shelf front, with the topographic high of the continental shelf acting as a former grounding line position.

Sediment core records in this area are sparse and are not conclusive as to whether grounded ice covered the entire continental shelf, as far as the continental slope (approximately the 1000 m contour in Fig. 1), during the Last Glacial Maximum (LGM: 23 - 19 ka BP). It is clear that ice has been grounded on the continental shelf break of DML during previous glacial periods (Grobe & Mackensen, 1992), however sediment cores from the continental shelf, in front of Ekström Ice Shelf, were not deep enough to provide material from the LGM. The Holocene aged sediments they contained (11.7 ka BP to present), were likely deposited beneath an ice shelf (Grobe & Mackensen, 1992), close to the grounding line. Hillenbrand et al. (2014) suggest two different LGM ice extent scenarios, the first with grounded ice extending to the continental shelf break and the second with ice grounded at around 25km upstream of the current shelf edge. The extent of the trough in our new bathymetry suggest that grounded ice reached to at least the current ice-shelf front in the past, possibly at the LGM.

The seismic line extending from the main grid to the south, shows a sea floor that continues to deepen all the way to the current grounding line (Fig. 3c, A-A'). The general trend of a retrograde slope within the trough would have allowed for rapid ice retreat after the LGM, until a stable point (topographic high) was reached. There are a number of topographic highs along the ice flow direction, which could indicate former grounding line positions. Particularly prominent is the topographic high at 100 km along profile A-A', which is around 200 m above the surrounding sea floor. We suggest that this is a former grounding line position, although current bathymetry measurements in this region do not extend laterally to confirm the extent of this feature. Upstream of this high is an overdeepening, reaching 1100 m depth and sitting around 10 km downstream of the current grounding line. Overdeepenings are commonly formed in areas of convergent flow, where ice velocities and erosional potential are high (Patton et al., 2016). The location of this overdeepening is at the convergence of two tributaries, with higher modern-day ice flow velocities than the surrounding ice (Neckel et al., 2012). When ice was thicker and grounded further seaward, the overdeepend area would have been a junction between these two tributaries, where a deep basin could have been eroded. Overdeepenings typically terminate in sills, where ice flow becomes less constrained, which could explain the origin of the topographic high we observe at 100 km along profile A-A'. Three smaller topographic highs at 35 km, 45 km and 60 km along the profile A-A' are around 50 m in height. These are also possible former shorter-term grounding positions, hinting at episodic retreat of the ice towards it's current grounding line.

4 Conclusions

We have presented new bathymetry data from under the Ekström Ice Shelf, Dronning Maud Land, Antarctica. The use of seismic vibroseis surveys proved an effective method for collecting this high resolution data across large areas of the ice shelf. As a result, the Ekström Ice Shelf cavity is currently one of the best mapped in Antartica. The discovery of a deep trough under Ekström Ice Shelf is the second example of such

a feature under a DML ice shelf, after the neighbouring Fimbul Ice Shelf. An 850 m deep trough is also seen at the shelf front of the Roi Baudouin Ice Shelf (Favier et al., 2016). Although it is not yet known whether this continues beneath the shelf itself, it further suggests that the bathymetry we see at Ekström and Fimbul is likely characteristic of other DML ice shelves. While these ice shelves are small, they are numerous and very little is known about the cavity geometry. Both current cavity geometry and knowledge of past ice dynamics are important to understand the future. The ice shelves of DML are known to play a key role in preconditioning the water-mass properties of the westward flowing boundary current, which affects the much larger Flicher-Ronne Ice Shelf and thus large portions of the West Antarctica Ice Sheet. Improved knowledge of ice-shelf cavities is a key step towards better understanding the fate of marine terminating ice sheets.

Acknowledgments

Field work and data processing by ECS since 2016 was funded through the AWI-BGR Sub-EIS-Obs Project. ECS was additionally funded through the DFG Cost S2S project, grant number EI672/10-1 in the framework of the priority programme "Antarctic Research with comparative investigations in Arctic ice areas", RD by the grant MA 3347/10-1 and EH 329/13-1. The field work of A. Lambrecht in 2010 was kindly supported by the Institute of Meteorology and Geophysics, University of Innsbruck, Austria. S. Berger was partly funded by the MIMO (Monitoring melt where Ice Meets Ocean) project, Belgian Science Policy contract Nos. SR/00/336. We thank R. Blenkner, J. Köhler, H. Schubert, J. Tell, B Ehlers, S. Hilmarsson and the staff at Neumayer Station III for logistical support. N. Koglin for discussion on borehole locations and geological constraints. The authors would like to thank C. Haas and J-L. Tison for loan on the CTD equipment and Emerson E&P Software, Emerson Automation Solutions, for providing licenses for the seismic software Paradigm, in the scope of the Emerson Academic Program. The initial idea for envisaging a geologic drilling underneath Ekström Ice Shelf was put forward by Y. Kristoffersen, who's stimulating creativity and technical support over the years the authors would like to acknowledge in particular. The gridded bathymetry data and CTD data are archived with PANGAEA (https://www.pangaea.de/), the doi for each data set will be provided on acceptance of the paper.

Author Contributions: All authors contributed to seismic target and profiling design, discussed the manuscript and contributed comments towards the final version. ECS designed and wrote the paper, performed fieldwork and led one field season, analysed and interpreted seismic data; TH analysed CTD data and provided the oceanographic component to the paper; DF and A Lambrecht performed seismic data acquisition and analysis, CM performed seismic data acquisition and led one field season, SB acquired and analysed CTD data and provided glaciological constrains for ice shelf processes, RD, TAE and CM contributed ice-flow modelling results and glaciological/geological constraints for data interpretation, CH was in charge of the seismic equipment and processed seismic data, GK, CG, A Läufer and RT provided geological constraints for data interpretation, FW prepared and coordinated the hot water drilling system, RG led one field season and performed cavity sampling, OE coordinated and implemented the seismic field work, led three field seasons, performed seismic and CTD data acquisition. GK, CG, A Läufer, RT, FW and OE are project Co-PIs, designed financial support and project implementation, CG and OE administratively coordinated the project. The trans-disciplinary science component is based on Kuhn and Gaedicke (2015).

References

Arndt, J. E., Schenke, H. W., Jakobsson, M., Nitsche, F. O., Buys, G., Goleby, B., ... Wigley, R. (2013). The international bathymetric chart of the Southern Ocean (IBCSO) version 1.0-A new bathymetric compilation cov-

ering circum-Antarctic waters. *Geophys. Res. Lett.*, *40*(12), 3111–3117. doi: 10.1002/grl.50413

Berger, S., Drews, R., Helm, V., Sun, S., & Pattyn, F. (2017). Detecting high spatial variability of ice shelf basal mass balance , Roi Baudouin Ice Shelf , Antarctica. *The Cryosphere*, *11*, 2675–2690. doi: 10.5194/tc-11-2675-2017

Brisbourne, A. M., Smith, A. M., King, E. C., Nicholls, K. W., Holland, P. R., & Makinson, K. (2014, jan). Seabed topography beneath Larsen C Ice Shelf from seismic soundings. *The Cryosphere*, *8*, 1–13. doi: 10.5194/tc-8-1-2014

Cochran, J. R., Jacobs, S. S., Tinto, K. J., & Bell, R. E. (2014). Bathymetric and oceanic controls on Abbot Ice Shelf thickness and stability. *The Cryosphere*, *8*, 877–889. doi: 10.5194/tc-8-877-2014

Dupont, T. K., & Alley, R. B. (2005). Assessment of the importance of ice-shelf buttressing to ice-sheet flow. *Geophys. Res. Lett.*, *32*(4), 1–4. doi: 10.1029/2004GL022024

Eisen, O., Hofstede, C., Diez, A., Kristoffersen, Y., Lambrecht, A., Mayer, C., ... Hilmarsson, S. (2015). On-ice vibroseis and snowstreamer systems for geoscientific research. *Polar Science*, *9*(1), 51–65. doi: 10.1016/j.polar.2014.10.003

Fahrbach, E., Rohardt, G., Schröder, M., & Strass, V. (1994). Transport and structure of the weddell gyre. *Annales Geophysicae*, *12*(9), 840–855. doi: 10.1007/s00585-994-0840-7

Favier, L., Pattyn, F., Berger, S., & Drews, R. (2016). Dynamic influence of pinning points on marine ice-sheet stability: A numerical study in Dronning Maud Land, East Antarctica. *The Cryosphere*, *10*(6), 2623–2635. doi: 10.5194/tc-10-2623-2016

Förste, C., Schmidt, R., Stubenvoll, R., Flechtner, F., Meyer, U., König, R., ... Esselborn, S. (2008). The GeoForschungsZentrum Potsdam/Groupe de Recherche de Gèodésie Spatiale satellite-only and combined gravity field models: EIGEN-GL04S1 and EIGEN-GL04C. *J. Geodesy*, *82*(6), 331–346. doi: 10.1007/s00190-007-0183-8

Fretwell, P., Pritchard, H. D., Vaughan, D. G., Bamber, J. L., Barrand, N. E., Bell, R., ... Zirizzotti, A. (2013, feb). Bedmap2: improved ice bed, surface and thickness datasets for Antarctica. *The Cryosphere*, *7*(1), 375–393. doi: 10.5194/tc-7-375-2013

Gade, H. G. (1979). Melting of Ice in Sea Water: A Primitive Model with Application to the Antarctic Ice Shelf and Icebergs. *J. Phys. Oceanogr.*, *9*(1), 189–198. doi: 10.1175/1520-0485(1979)009⟨0189:moiisw⟩2.0.co;2

Goldberg, D. N., Gourmelen, N., Kimura, S., Millan, R., & Snow, K. (2019). How Accurately Should We Model Ice Shelf Melt Rates? *Geophys. Res. Lett.*, *46*(1), 189–199. doi: 10.1029/2018GL080383

Grobe, H., & Mackensen, A. (1992). Late Quaternary climatic cycles as recorded in sediments from the Antarctic continental margin. *Antarctic Research Series - AGU*, *56*, 349–376. doi: 10.1029/ar056p0349

Hattermann, T. (2018). Antarctic thermocline dynamics along a narrow shelf with easterly winds. *J. Phys. Oceanogr.*, *48*(10), 2419–2443. doi: 10.1175/JPO-D-18-0064.1

Hattermann, T., Nst, O. A., Lilly, J. M., & Smedsrud, L. H. (2012). Two years of oceanic observations below the Fimbul Ice Shelf, Antarctica. *Geophys. Res. Lett.*, *39*(12), 1–6. doi: 10.1029/2012GL051012

Hattermann, T., Smedsrud, L. H., Nøst, O. A., Lilly, J. M., & Galton-Fenzi, B. K. (2014). Eddy-resolving simulations of the Fimbul Ice Shelf cavity circulation: Basal melting and exchange with open ocean. *Ocean Modelling*, *82*, 28–44. doi: 10.1016/j.ocemod.2014.07.004

Hellmer, H. H., Kauker, F., Timmermann, R., & Hattermann, T. (2017). The fate of the Southern Weddell sea continental shelf in a warming climate. *J. Climate*, *30*(12), 4337–4350. doi: 10.1175/JCLI-D-16-0420.1

Heywood, K. J., Locarnini, R. A., Frew, R. D., Dennis, P. F., & King, B. A. (1994). Transport and water masses of the Antarctic Slope Front system in the Eastern Weddell Sea. *Antarctic Research Series*, *75*, 203–214. doi: 10.1029/ar075p0203

Hillenbrand, C.-d., Bentley, M. J., Stolldorf, T. D., Hein, A. S., Kuhn, G., Graham, A. G. C., ... Sugden, D. E. (2014). Reconstruction of changes in the Weddell Sea sector of the Antarctic Ice Sheet since the Last Glacial Maximum. *Quat. Sci. Rev.*, *100*, 111–136. doi: 10.1016/j.quascirev.2013.07.020

Hoppmann, M., Nicolaus, M., Paul, S., Hunkeler, P. A., Heinemann, G., Willmes, S., ... Gerdes, R. (2015). Ice platelets below weddell sea landfast sea ice. *Ann. Glaciol.*, *56*(69), 175–190. doi: 10.3189/2015AoG69A678

Howat, I. M., Morin, P. J., Porter, C. C., & Noh, M. J. (2019). The Reference Elevation Model of Antarctica, V1. *The Cryosphere*, *13*, 665–674. doi: 10.7910/DVN/SAIK8B

IOC, SCOR, & IAPSO. (2010). *The International Thermodynamic Equation of Seawater2010: Calculation and Use of Thermodynamic Properties, Intergovernmental Oceanographic Commission, Manuals and Guides No. 56.* University of Southampton: UNESCO.

IPCC. (2019). *IPCC Special Report on the Ocean and Cryosphere in a Changing Climate [H.-O. Pörtner, Roberts, D. C., Masson-Delmotte, V., Zhai, P., Tignor, M., Poloczanska, E., Mintenbeck, K., Nicolai, M., Okem, A., Petzold, J. Rama, B. Weyer, N. (eds.)]* (Tech. Rep.). doi: https://www.ipcc.ch/report/srocc/

Kobarg. (1988). The tide-dependent dynamics of the Ekstroem Ice Shelf, Antarctica. *Berichte zur Polar- und Meeresforschung*, *50*.

Kristoffersen, Y., Hofstede, C., Diez, A., Blenkner, R., Lambrecht, A., Mayer, C., & Eisen, O. (2014). Reassembling Gondwana: A new high quality constraint from vibroseis exploration of the sub-ice shelf geology of the East Antarctic continental margin. *J. Geophys. Res. Solid Earth*, *119*, 9171–9182. doi: 10.1002/2014JB011479

Kuhn, G., & Gaedicke, C. (2015). A plan for interdisciplinary process.studies and geoscientific observations beneath the Eckstroem Ice Shelf (Sub-EIS-Obs). *Polarforschung*, *84*(2), 99–102.

Lindbäck, K., Moholdt, G., Nicholls, K. W., Hattermann, T., Pratap, B., Thamban, M., & Matsuoka, K. (2019). Spatial and temporal variations in basal melting at Nivlisen ice shelf , East Antarctica , derived from phase-sensitive radars. *The Cryosphere*, *13*, 2579–2595. doi: 10.5194/tc-13-2579-2019

McDougall, T. J., & Barker, P. M. (2011). *Getting started with TEOS-10 and the Gibbs Seawater (GSW) Oceanographic Toolbox,*. SCOR/IAPSO WG127.

Meijers, A. J. S., Meredith, M. P., Abrahamsen, E. P., Morales Maqueda, M. A., Jones, D. C., & Naveira Garabato, A. C. (2016). Wind-driven export of Weddell Sea slope water. *J. Geophys. Res. Oceans*, *121*, 7530–7546. doi: 10.1002/2016JC011757

Meredith, M. P., Gordon, A. L., Naveira Garabato, A. C., Abrahamsen, E. P., Huber, B. A., Jullion, L., & Venables, H. J. (2011). Synchronous intensification and warming of Antarctic Bottom Water outflow from the Weddell Gyre. *Geophys. Res. Lett.*, *38*(3), 2–5. doi: 10.1029/2010GL046265

Milillo, P., Rignot, E., Rizzoli, P., Scheuchl, B., Mouginot, J., Bueso-Bello, J., & Prats-Iraola, P. (2019). Heterogeneous retreat and ice melt of Thwaites Glacier, West Antarctica. *Sci. Adv.*, *5*(1), eaau3433. doi: 10.1126/sciadv.aau3433

Neckel, N., Drews, R., Rack, W., & Steinhage, D. (2012). Ice Shelf , Antarctica , estimated from Basal melting at the Ekstr om mass flux divergence. *Ann. Glaciol.*, *53*(60), 294–302. doi: 10.3189/2012AoG60A167

Nicholls, K. W., Abrahamsen, E. P., Buck, J. J. H., Dodd, P. A., Goldblatt, C.,

Griffiths, G., ... Wilkinson, J. P. (2006). Measurements beneath an Antarctic ice shelf using an autonomous underwater vehicle. *Geophys. Res. Lett.*, *33*, 2–5. doi: 10.1029/2006GL025998

Nøst, O. A. (2004). Measurements of ice thickness and seabed topography under the Fimbul Ice Shelf, Dronning Maud Land, Antartica. *J. Geophys. Res.*, *109*, 1–14. doi: 10.1029/2004JC002277

Nøst, O. A., Biuw, M., Tverberg, V., Lydersen, C., Hattermann, T., Zhou, Q., ... Kovacs, K. M. (2011). Eddy overturning of the Antarctic Slope Front controls glacial melting in the Eastern Weddell Sea. *J. Geophys. Res. Oceans*, *116*(11), 1–17. doi: 10.1029/2011JC006965

Padman, L., Erofeeva, S. Y., & Flicker, H. A. (2008). Improving Antarctic tide models by assimilation of ICESat laser altimetry over ice shelves. *Geophys. Res. Lett.*, *35*, 1–5. doi: 10.1029/2008GL035592

Paolo, F. S., Fricker, H. A., & Padman, L. (2015). Volume loss from Antarctic ice shelves is accelerating. *Science*, *348*(6232), 327–331. doi: 10.1126/science.aaa0940

Patton, H., Swift, D. A., Clark, C. D., Livingstone, S. J., & Cook, S. J. (2016). Distribution and characteristics of overdeepenings beneath the Greenland and Antarctic ice sheets : Implications for overdeepening origin and evolution. *Quat. Sci. Rev.*, *148*, 128–145. doi: 10.1016/j.quascirev.2016.07.012

Pattyn, F., Favier, L., Sun, S., & Durand, G. (2017). Progress in Numerical Modeling of Antarctic Ice-Sheet Dynamics. *Current Climate Change Reports*, *3*(3), 174–184. doi: 10.1007/s40641-017-0069-7

Pritchard, H. D., Ligtenberg, S. R., Fricker, H. A., Vaughan, D. G., Van Den Broeke, M. R., & Padman, L. (2012). Antarctic ice-sheet loss driven by basal melting of ice shelves. *Nature*, *484*(7395), 502–505. doi: 10.1038/nature10968

Rignot, E., Jacobs, S., Mouginot, J., & Scheuchl, B. (2013). Ice-Shelf Melting Around Antarctica. *Science*, *341*(6143), 266–270. doi: 10.1126/science.1235798

Rosier, S. H., Hofstede, C., Brisbourne, A. M., Hattermann, T., Nicholls, K. W., Davis, P. E., ... Corr, H. F. (2018). A New Bathymetry for the Southeastern Filchner-Ronne Ice Shelf: Implications for Modern Oceanographic Processes and Glacial History. *J. Geophys. Res. Oceans*, *123*(7), 4610–4623. doi: 10.1029/2018JC013982

Thompson, A. F., Stewart, A. L., Spence, P., & Heywood, K. J. (2018). The Antarctic Slope Current in a Changing Climate. *Rev. Geophys.*, *56*(4), 741–770. doi: 10.1029/2018RG000624

Timmermann, R., & Hellmer, H. H. (2013). Southern Ocean warming and increased ice shelf basal melting in the twenty-first and twenty-second centuries based on coupled ice-ocean finite-element modelling. *Ocean Dyn.*, *63*(9-10), 1011–1026. doi: 10.1007/s10236-013-0642-0

Tinto, K. J., Padman, L., Siddoway, C. S., Springer, S. R., Fricker, H. A., Das, I., ... Bell, R. E. (2019). Ross Ice Shelf response to climate driven by the tectonic imprint on seafloor bathymetry. *Nat. Geosci.*, *12*(June). doi: 10.1038/s41561-019-0370-2